

# Panoramic UAV Surveillance System based on Structure-free Fisheye Camera Array

**Abstract**—In recent years, Unmanned Aerial Vehicles(UAVs) have been explosively developed, but the use of UAVs in civilian miniature exposed by disorder and security risks are increasingly triggered community concern and worry. Therefore, the location, tracking and monitoring UAVs in key regions, is of great significance. This paper presents a novel panoramic UAV surveillance system, which is based on an unique structure-free fisheye camera array, and has the capability of 3D detection and tracking multiple UAVs in a very wide field of view. The main characteristics of this work include: (1) Construct a ground random fisheye camera array based UAV surveillance system; (2) Design a robust Near Infrared Laser based self-calibration module and algorithm for arbitrary layout of camera array; and (3) Present a set of multi-target detection, tracking and 3D localization algorithm based on the fisheye camera array. The system has been tested in various challenging scenarios, include multiple UAVs with significant appearance and scale changes, and even bad weather conditions. Extensive experimental results, both qualitative and quantitative, demonstrate that the robustness and superiority of the proposed system.

**Index Terms**—UAV, Structure-free Fisheye Camera Array, Surveillance System

## I. INTRODUCTION

WITH the maturity of UAVs technology, the UAVs manufacturing costs and use-costs are decreasing, large numbers of UAVs research and development, manufacturing and application company boost the popularity of civilian UAV [1]. Small and medium UAVs as the representative of civil unmanned aerial system is set off the development boom in the world, but the use of UAVs in civilian miniature exposed by disorder and security risks [2], such as stealing private information within the area, putting hazardous materials and etc. Which are increasingly triggered community concern and worry. Consequently, anti-UAV surveillance is a relatively new and largely unexplored area, which technology is of great significance and value.

From a technical view, there are several major types of anti-UAV surveillance technologies, such as signal interference, radar detection, integrated technology and so on. Signal jamming technology can affect the UAV's GPS signal receiver, where the control and navigation information is disturbed by strong interference. For example, an electromagnetic gun, which makes the auto-driving system or the communication system of UAVs become invalid. Radar detection technology has the ability of powerful detection of small and low speed targets. Swedish “GIRAFFE” radar system, it's cross section is accurate to 0.001 square meters. Italy Finmeccanica Selex ES company demonstrates its “falcon shield” UAV system. The system can locate, identify and control long-range small UAVs. Integrated technology has the ability to be more powerful.

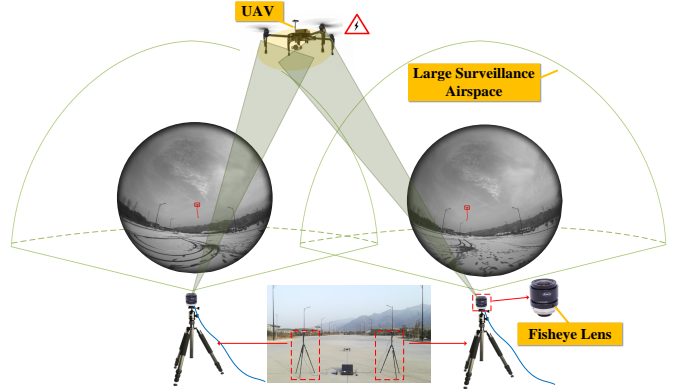


Fig. 1. Architecture of the panoramic UAV surveillance system based on structure-free fisheye camera array.

British anti-UAV defense system AUDS, which can detect, track and destroy small and large UAVs. Although the existing anti-UAV technologies and systems can serve as a good inspiration for the research on UAVs surveillance, there are still many issues open to solutions. First of all, UAVs are generally small in size and weight, and they appear suddenly, which makes them hard to detect. Second, the integration of artificial intelligence and advanced materials into the design of UAVs will significantly improve their capability in stealth. Third, the majority of existing anti-UAV technologies are designed for specific UAVs or scenarios via few technical methods, which limits their applications and generalization.

In order to acquire accurate position of UAV, many high precision measuring sensors, such as laser range scanners [3], [4] have been used. With the rapid development of intelligent vision technology and visual sensors, such as monocular cameras [5], [6], stereo cameras [7], [8], and RGB-D sensors [9], [10], which have become the core part of the UAV monitoring system [11], [12]. Martinez et al. [13] design a trinocular system, which is composed of three FireWire cameras fixed on the ground, to estimate the vehicle's position and orientation by tracking the markers on the UAV. Pebrianti et al. [14] propose a ground-based stereo vision system to estimate the three dimensional position of a quadrotor. Although those systems achieve satisfied results, they can only be used in the indoor environment due to the limited distance measurement. In order to enlarge the surveillance range as well as the monitoring field of view(FOV), some systems and solutions have been proposed in recent years [15]–[20]. Kong et al. [21], [22] construct a system that mounted two separate sets of pan-tilt unit integrated with visible light camera on both sides of the runway, which is able to detect the fixed-wing UAV at about 600 meters. Tao et al. [23] present a high accuracy large scale outdoor camera array calibration method in the work in 2015. Through integrating the infrared camera and laser

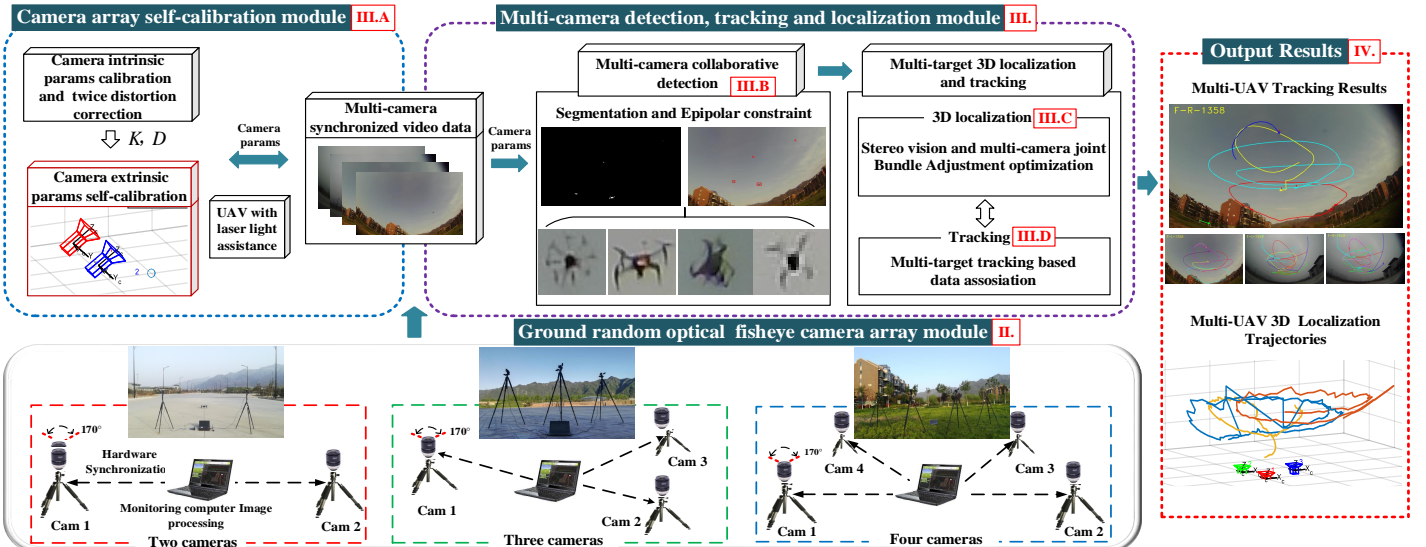


Fig. 2. Overall structure and algorithm flow of proposed ground random fisheye camera array anti-UAVs surveillance system.

lights, their system can robustly detect and guide UAV landing safely within a range of 800 meters. Although those systems [21]–[23] achieve good performance on cooperative target, they cannot be applied to non cooperative UAV surveillance. Moreover, due to the small field of view, they cannot be used for large area UAV monitoring tasks directly.

In view of the UAV surveillance system, the ability of wide-angle monitoring and high precision localization are the two most important aspects. Although the system's view angle can be enlarged by using multiple cameras, it will substantially increase the system complexity in the meantime, for instance, the structure design, multi-camera joint calibration, and data synchronization. Different with the traditional monitoring camera, fisheye camera is an attractive choice as it offer very large field of view. Therefore in this work, we select fisheye camera as the core visual sensor to build a novel camera array based UAV optical surveillance system. The contributions of this paper are three main aspects:

- Constructing a novel type of real-time panoramic UAV surveillance system based on structure-free fisheye camera array for the first time, to the best our knowledge. The fisheye camera array ensures large monitoring FOV, and the free system structure is convenient for rapid deployment and flexible configuration.
- Designing a robust Near Infrared Laser based self-calibration module and algorithm for arbitrary layout of camera array without any other markers, especially in the environment with low texture or solid color background. A large number of experiments prove its effectiveness and high efficiency for different structure of camera array.
- Presenting an intelligent synergetic UAV detection, 3D localization and tracking algorithm based on fisheye camera array. Extensive real flight experiments in complicated and challenging scenarios, include four different types of UAV, large scale changes and the interleaving of UAV during the flight, demonstrate the effective and efficiency of the algorithm.

This remainder of this paper is organized as follows. The

architecture configuration of the panoramic UAV surveillance system is presented in Section II. Section III describe the detailed algorithm of the proposed system. Section IV verify the proposed system through several experiments, Finally, our conclusions are given in Section V.

## II. ARCHITECTURE CONFIGURATION OF PANORAMIC UAV SURVEILLANCE SYSTEM

This paper mainly focus on the anti-UAV surveillance mission based on structure-free fisheye camera array. The complete experimental setup is shown in Fig. 1. The system overall framework is shown in Fig. 2, which is mainly consist of three main module: (1) ground structure-free fisheye camera array module, (2) camera array fast self-calibration module, and (3) multi-camera synergetic detection, 3D localization and tracking module for multi-UAV.

### A. Structure-free Fisheye Camera Array Imaging System

**Fisheye optical imaging module:** In order to cover the larger monitoring area, we construct a novel panoramic UAV surveillance system based on structure-free fisheye camera array. The system is mainly consist of several fisheye cameras, which are fixed on the pan-tilt units. The pan-tilt units are mounted on tripods, and the entire device can be rotated, which helps to quickly adjust the camera angle. We select two kinds of cameras in experiment, which are shown in Table I. The first imaging module combines the infrared camera of pointGrey GS3-U3-41C6NIR-C and Kowa LM4NCL fisheye lens. The camera has the powerful frame rate acquisition capability  $2048 \times 2048$  pixels at 90 fps with a large FOV 150°. The second imaging module is the integrated USB module camera, which focal length is 3.8 mm with a wide FOV up to 170°. The cameras use the USB3.0 data interface to guarantee the requirement of high speed image synchronization acquisition, which captures the images by 30 frames per second with a resolution  $1920 \times 1080$  pixels. The more detailed camera and lens parameters are shown in Table I, the parameters of above two cameras meet the need of the proposed system.

TABLE I  
THE CAMERA AND FISHEYE LENS PARAMETERS

Camera/Lens	Specification	Parameter
pointGrey	Sensor	CMV4000-3E12
	Max resolution	2048 × 2048 pixels
	Max frame rate	90 fps
	Working voltage	DC 4.5v
	Focal length	3.5 mm
	Angle of view	150°
Kowa LM4NCL	TV distortion	-28.0%
	Weight	60 g
USB Camera	Focal length	3.8 mm
	Max resolution	1920 × 1080 pixels
	Max frame rate	30 fps
	Angle of view	170°

**Structure-free architecture:** In the experiment, we design diversified camera array structures ranging from two to four cameras with random positions, which is shown in the lower left corner of Fig. 2. Each camera is coupled to the entire camera array network as an independent node, and the images of all cameras are introduced into the ground processor by data synchronization. The camera array ensure large FOV and the stability and robustness of the system, and the free structure is convenient for rapid deployment and flexible configuration.

### B. Assist Self-calibration UAV and Sky-Ground Data Link

**Assist self-calibration UAV:** In order to complete the self calibration of the camera array, we use the airborne laser lamp to assist the calibration and the UAV setup is shown in Fig. 3. The operation details will be explained in the Section III. In the experiment, all the flight experiment data collection via manual flight or remote control with the aid of our GPS waypoint navigation system. In order to ensure the robustness of target detection, the flying altitudes are less than 100 meters.

**Sky-Ground data link module:** Our ground localization computer is equipped with Intel Core i7 2.4 GHz processor and 8 GB DDR3. The wireless transmission module ensures the effective data communication between sky and ground, which with more than 1 km transmission capability in unshielded environment. The UAV equipped with an on-board computer Manifold to achieve real-time data forwarding, the complete UAV setup is shown in Fig. 3. The data link not only assistants the self-calibration process of the camera array, but also plays an important role in the precision contrast in the UAVs localization experiment.

## III. GROUND RANDOM FISHEYE CAMERA ARRAY ANTI-UAVS SURVEILLANCE SYSTEM

### A. Fisheye Lens Description and Self-calibration

We adopt the fisheye camera array method, and how to accurately calibrate the fisheye camera array internal and external parameters is our first task. The accuracy of the camera parameters directly determines the localization accuracy.



Fig. 3. The UAV setup for fisheye camera array self-calibration.

**Fisheye lens twice distortion correction:** The fisheye lens is an ultra-wide lens and can provide a wide field of view, both horizontally and vertically, which imaging model is shown in Fig. 4. The images obtained with such the lens are highly distorted. The most popular are the equiangular fisheye lens: the angular resolution provided by the lens is constant. They are characterized by the equality  $r = f\theta$ , where  $f$  is the focal length of the lens,  $\theta$  is the incoming ray angle and  $r$  is the projection of the ray on the image plane. This relationship is a theoretical one. In reality, there are deviation from this equality due to imperfection in lens production and assembly.

In order to accurately calibrate the fisheye cameras intrinsic parameters and remove the distortion, twice distortion correction process have been carried out. For the first calibration, we use the OPENCV toolbox of the fisheye camera model, which derived a projection function that can cope with any type of ultra-wide lens. It is briefly described that

$$\theta_d = \theta(1 + k_1\theta^2 + k_2\theta^4 + k_3\theta^6 + k_4\theta^8) \quad (1)$$

We can easily get the intrinsic parameters  $K_i$  and distortion coefficient  $D_i(k_1, k_2, k_3, k_4)(i = 1, 2, 3\dots)$  of each camera. The first correction result

$$p'(u', v') = K \cdot \theta_d \begin{bmatrix} \cos \varphi \\ \sin \varphi \end{bmatrix} \quad (2)$$

where  $p'(u', v')$  is the first corrected image coordinates,  $\theta_d$  is defined in (1),  $\varphi$  is the angle between the radial direction and the  $x$ -axis,  $K$  is the camera intrinsic parameters.

As the results shown, there are still some local residuals exist, so we carry out the second fine calibration. In the second calibration, we calibrate the images after first correction, using a pinhole camera model. The  $p''(u'', v'')$  can be defined

$$\begin{cases} u'' = u' + (u' - c_x) \cdot k \cdot r^2 \\ v'' = v' + (v' - c_y) \cdot k \cdot r^2 \end{cases} \quad (3)$$

where  $p''(u'', v'')$  defines the second correction image coordinate,  $k$  is the radial distortion coefficient by second calibration,  $(c_x, c_y)$  is the optical center, and  $r$  is the distance to the optical

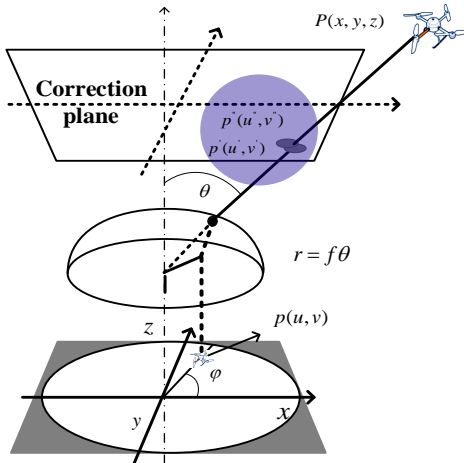


Fig. 4. Fisheye camera model. The 3-D  $P$  is imaged at  $p$  by fisheye camera, the  $p'$  and  $p''$  are the first and second correction result, respectively.

center. The twice correction result shown in Fig. 5, and the final calibration accuracy is less than 0.015 pixel.

**Camera array extrinsic parameters self-calibration:** As for the extrinsic parameters between camera array, the conventional calibration methods are mostly based on calibration plates or markers in the scene. It is difficult to place any available markers in the airspace, so the methods are not valid for the case of upward field of camera view.

In order to solve the calibration problem, this paper proposes a novel and generic camera array self-calibration method, which is mainly based on a laser light mounted on a UAV, the setup is shown in Fig. 3. The precision of the light point detection determines the accuracy of the final calibration, so how you accurately detect the laser point is critical. Firstly, we adopt the laser light as our collaborative targets, which can be observed of long distance and large angle. Second, we conduct morphological processing on original image. The laser light imaging result is shown in Fig. 6, and the energy distribution is approximated by a Gauss model, which cross section approximate ellipse. Finally, we adopt a multilevel elliptic fitting algorithm to solve the center of light point, the detection result is shown in Fig. 6(c).

The camera array self-calibration algorithm mainly includes several steps. First of all, we extract and correct the image coordinates of the light points, and the synchronous GPS data of UAV is collected. Next, estimating the transform between cameras by 2D-2D corresponding points using ransac method, and the 3D coordinates of the light points are triangulated and further optimized by Bundle Adjustment. Finally, the transform between camera and world coordinate is estimated by the vision and GPS data, and we get the the final extrinsic parameters. The algorithmic details are shown in Algorithm 1. The projection matrix  $P_i$  of each camera:

$$P_i = K_i \cdot T_i = K_i \cdot R_i + t_i \quad (4)$$

where  $K_i$  and  $T_i$  are the intrinsic and extrinsic parameters of each camera, respectively.

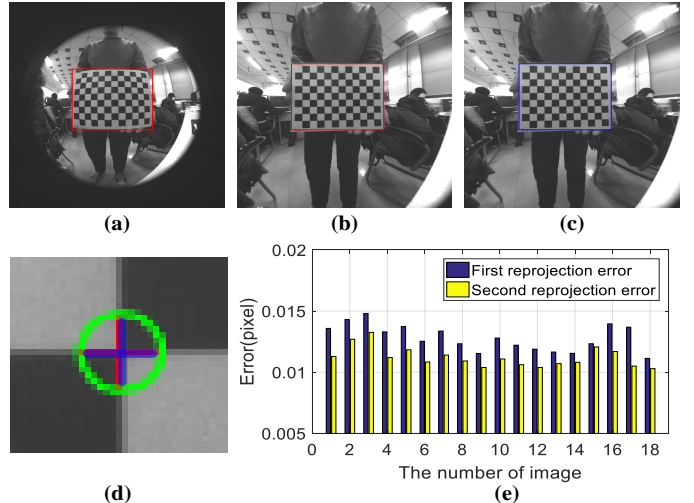


Fig. 5. Distortion correction of fisheye camera. (a) original distort image. (b) first undistort result. (c) seond undistort result. (d) corner reprojeciton result. (e) reprojection pixel error.

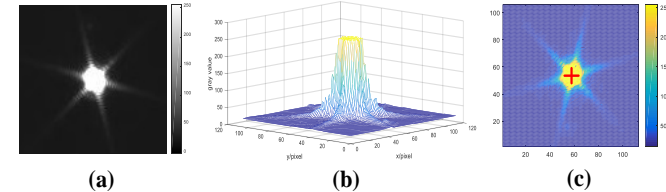


Fig. 6. The laser light imaging energy. (a) light point of the laser lamp. (b) light point energy distribution. (c) interpolated ROI.

### B. Multi-camera Collaborative Multi-target Detection

As shown in Fig. 2, our fisheye cameras are installed on the tripod with static and upward camera view. In order to get good foreground targets, we use the ViBe [24] foreground extraction method in this paper, which performs robust and produces complete segmentation results shown in Fig. 8. The algorithm can extract multi-UAV completely under different sizes, especially those weak and small targets.

We regard the image centroid coordinate of each cluster as the coordinate of the candidate target in the image. The pixel distance is defined as:

$$f_{pd}(p_i, p_j) = \sqrt{(p_i^x - p_j^x)^2 + (p_i^y - p_j^y)^2} \quad (5)$$

where  $p_i$  and  $p_j$  are image pixels,  $(p_i^x, p_i^y)$  and  $(p_j^x, p_j^y)$  are pixel coordinate of  $p_i$  and  $p_j$  respectively.

To determine the corresponding relationship of the candidate targets and remove the false targets, epipolar geometry constraints between the two cameras are used. Epipolar geometry between the two cameras refers to the inherent projective geometry between the views. It only depends on the camera intrinsic parameters and the relative pose of the two cameras. Thus, after the target is detected on the two cameras independently, epipolar geometry constraints between the cameras can be used to get data association results. In this way, the corresponding relationship of the candidate targets are confirmed and parts of false targets are removed.

Define  $I_1 = \{x_1^1, x_2^1, \dots, x_m^1\}$  and  $I_2 = \{x_1^2, x_2^2, \dots, x_n^2\}$  as the detection results of the first and second camera. The duty of the data association is to find the corresponding relationship

**Algorithm 1** Camera Array Self-calibration Algorithm Flow.

**Require:** The set of ground random camera array,  $C_n$ ; The real distance of offline measurement between the  $i$  camera and the reference camera  $C_r$ ,  $D_r^i$ ; The GPS data of the origin of world coordinates,  $G_0$ ; The number of the pairwise points,  $N_{points}$ ;

**Ensure:** The rotation and translation matrix to the world coordinates of cameras,  $T_n(R|t)$ ;

- 1: Synchronize the images of each camera  $I_i^j$ , and the GPS data of the UAV  $G_j$ ;
- 2: **while** ( $j \leq N_{points}$ ) **do**
- 3:   Extracting coordinates of light points  $p_i^j(u, v)$ ;
- 4:   Correcting the light point coordinate  $\bar{p}_i^j(u, v)$ ;
- 5:   Calculating the 3D coordinate of the light point  $P_{gps}^j = F(G_j, G_0)$ ;
- 6: **end while**
- 7: Estimating the essential matrix  $E_n$  by 2D-2D corresponding points using ransac method;
- 8: Calculating the relative Transform  $t_n$  from  $E_n$  by SVD, and recover the scale by the  $D_r^n$ ;
- 9: Triangulating the  $N_{inlier}$  3D coordinates of the laser points  $P_{vision}$ ;
- 10: BA optimization, minimize the re-projection error between all cameras  $\min \sum_{i=1}^n \sum_{j=1}^{N_{inlier}} (P_{vision}^j, \bar{p}_i^j(u, v), t_n, K_i)$ ;
- 11: Estimating the transform  $t_{c2w}$  by the 3D points of vision and GPS, and finally get the  $T_n = t_{c2w} \cdot t_n$ ;
- 12: **return**  $T_n$ ;

between  $x_i^1$  and  $x_j^2$ . Distance measurement is obtained by the symmetric transfer error between  $x_i^1$  ( $i = 1, 2, \dots, m$ ) and  $x_j^2$  ( $j = 1, 2, \dots, n$ ), which can be defined as:

$$d(x_i^1, x_j^2) = d(x_i^1, F^T x_j^2) + d(x_j^2, F x_i^1) \quad (6)$$

where  $F$  is the fundamental matrix between the two cameras. The matching matrix between two images is:

$$D = \begin{bmatrix} d(x_1^1, x_1^2) & d(x_1^1, x_2^2) & \dots & d(x_1^1, x_n^2) \\ d(x_2^1, x_1^2) & d(x_2^1, x_2^2) & \dots & d(x_2^1, x_n^2) \\ \vdots & \vdots & \ddots & \vdots \\ d(x_m^1, x_1^2) & d(x_m^1, x_2^2) & \dots & d(x_m^1, x_n^2) \end{bmatrix} \quad (7)$$

The global optimal matching result is obtained by solving the matching matrix D using Hungarian algorithm, which is taken as the final detection result.

### C. 3D Localization and Motion Trajectories

As shown in Fig. 9, which clearly explain the architecture of the fisheye camera array optical localization system. The correct image is made using the calculation of inverse of fisheye imaging in Section III.A.

In Section III.A, we obtain the fisheye camera parameters including the intrinsic  $K_i$ , distortion coefficient  $D_i$  and extrinsic parameters(the relative rotation  $R$  and translation  $T$  between cameras). Supposing that the world coordinates of the UAVs are  $X = \{X_1, X_2, \dots, X_n\}$ , the camera projection matrix is  $P_i$ , which can easily calculate by the intrinsic

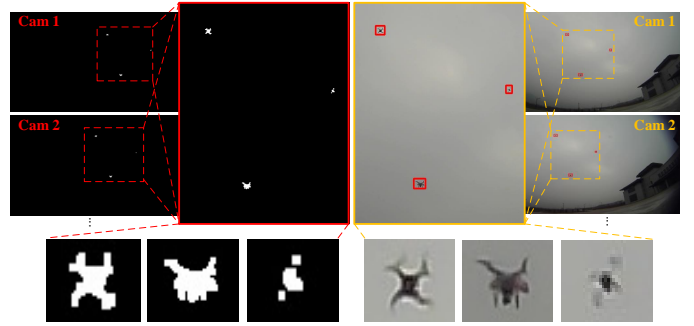


Fig. 8. Multi-camera collaborative detection based foreground segmentation and epipolar constrain.

and extrinsic parameters. For detection results, supposing the image coordinates of the UAVs are  $x_i = \{x_i^1, x_i^2, \dots, x_i^n\}$ . We explain the principle with two camera models. We obtain initial value of  $x_l$  and  $x_r$  by DLT algorithm firstly, and then we optimize the  $\hat{x}_l$  and  $\hat{x}_r$  using Levenberg-Marquardt's iterative non-linear optimization. Set  $x_l \cong P_l X$  and  $x_r \cong P_r X$ , with the homogeneous relations  $x_l P_l X = 0$  and  $x_r P_r X = 0$ . The above is linear equations with respect to  $X$ , which can be written as  $AX = 0$ . Each set of points corresponding to three equations which only two are linearly independent, therefore each point just gives two equations correspondingly with respect to  $X$ .

Since  $X$  is homogeneous coordinates, which only three degrees of freedom are scale-independent, however, the linear equation set  $AX = 0$  contains four equations, thus the above system is over-determined system. To find the approximate solution of the equation  $AX = 0$ , we can make it as a follow optimization with  $\|AX\| = 1$ .

$$\min_X \|AX\| \quad (8)$$

Primarily, we obtain the initial value of  $X$  by the above formula, and then optimize the value of  $X$  using the method of multiple view projective reconstruction by Bundle Adjustment. We get the final  $X$  by minimizing the follow function using LM iterative optimization algorithm.

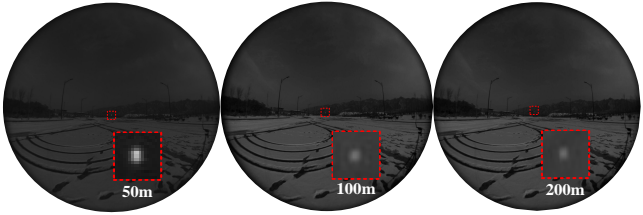
$$\min \sum_{i=1}^n v_i d(Q(X, I_i), x_i)^2 \quad (9)$$

Where  $I_i$  is the  $i$  camera frame, if there have imaging point on the  $I_i$  image, we set  $v_i = 1$ , otherwise set  $v_i = 0$ .  $Q(X, I_i)$  is the projection on the  $i$  camera frame and the  $d(Q(X, I_i), x_i)^2$  is the reprojection errors computed using the corresponding projection matrices.

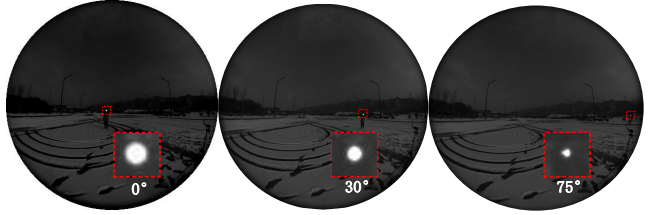
### D. Multiple Targets Tracking with 3D information fusion

The euclidean distance is used as the distance measurement in the 3D space. Define the historical target tracking result  $T_i^t$  ( $i = 1, 2, \dots, p$ ) and current localization result  $X_j^{t+1}$  ( $j = 1, 2, \dots, q$ ), the distance between them is computed by:

$$d(T_i^t, X_j^{t+1}) = \sqrt{(x_i^t - x_j^{t+1})^2 + (y_i^t - y_j^{t+1})^2 + (z_i^t - z_j^{t+1})^2} \quad (10)$$



(a) The comparision of the imaging at different distance.



(b) The comparision of the imaging at different angles.

Fig. 7. The Laser light imaging. (a) and (b) are the comparison of the imaging at different distance and different angles, respectively.

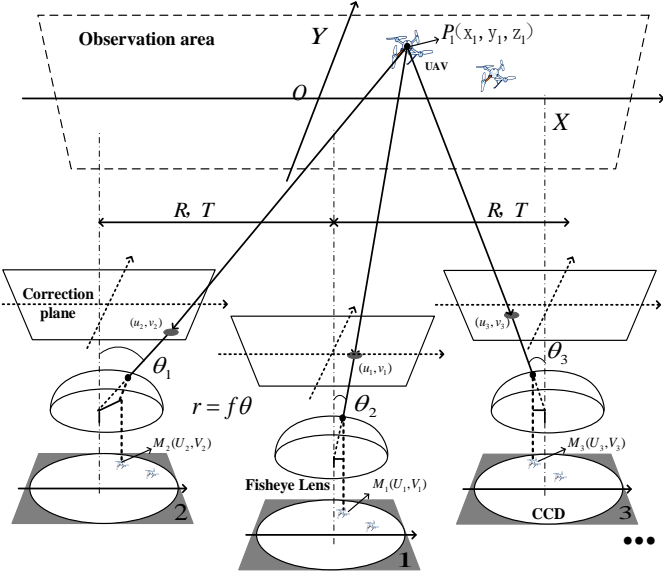


Fig. 9. Architecture of proposed ground fisheye camera array optical localization system.

where  $(x_i^t, y_i^t, z_i^t)$  and  $(x_j^{t+1}, y_j^{t+1}, z_j^{t+1})$  are space coordinates of  $T_i^t$  and  $X_j^{t+1}$ . Thus, the matching matrix between them is computed by:

$$D_t^{t+1} = \begin{bmatrix} d(T_1^t, X_1^{t+1}) & d(T_1^t, X_2^{t+1}) & \dots & d(T_1^t, X_q^{t+1}) \\ d(T_2^t, X_1^{t+1}) & d(T_2^t, X_2^{t+1}) & \dots & d(T_2^t, X_q^{t+1}) \\ \vdots & \vdots & \ddots & \vdots \\ d(T_p^t, X_1^{t+1}) & d(T_p^t, X_2^{t+1}) & \dots & d(T_p^t, X_q^{t+1}) \end{bmatrix} \quad (11)$$

The Hungarian algorithm is used to get the multiple targets tracking results from  $D_t^{t+1}$ .

#### IV. EXPERIMENTAL RESULTS

We have conducted a series of filed experiments to evaluate the structure-free fisheye camera array anti-UAV surveillance system. The experiments carry out in different environment and adopt various of UAVs with significant difference in appearance and size. In the following, multi-UAV experimental platform and camera array self-calibration experimental results are described in detail in Section IV.A. Section IV.B presents the multi-UAV detection, 3D localization and tracking result.

##### A. Multi-UAV Experimental Platfrom and Camera Array Self-calibration

In order to fully evaluate the proposed panoramic UAV surveillance system, multi-UAVs with different appearances

TABLE II  
FOUR TYPES OF MULTIPLE ROTOR AIRCRAFTS

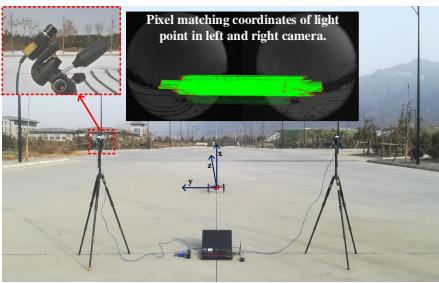
UAV name	Eight Rotor	M100	Pantom 3	Pantom 2
wheelbase(mm)	1133	650	350	350
weight(kg)	5.30	2.30	1.28	1.00
speed(km/h)	65	20	20	15



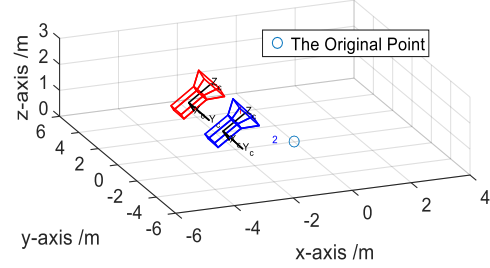
Fig. 10. Experimental UAVs with different appearances and sizes.

and sizes are employed to the experiments, and the details are shown in Table II and Fig. 10. An eight-rotor drone, the wheelbase of which is about 1133 mm and 5.30 kg weight with two standard batteries. The maximum speed is 65 km/h, equipped with DUAL SKY XM5015TE-5 motor. There are three quad-rotor vehicles, a DJI Matrix 100, the wheelbase of which is about 650 mm and 2.30 kg weight with one standard battery, a DJI Phantom professional 3 with 350 mm wheelbase and 1.28 kg weight, and a DJI Phantom 2 with 350 mm wheelbase and 1.00 kg weight.

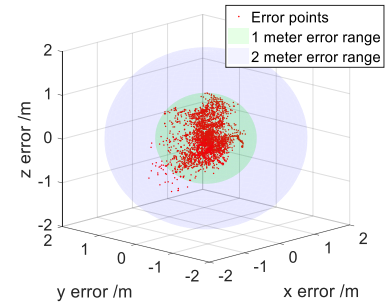
For the different structures of the fisheye camera array, we conduct a number of different experiments to verify the proposed self-calibration method. In our method, the most of the wrong matching and outlier points are removed by epipolar constraint, and in order to get a better calibration result, the UAV flies at different heights and distance which cover the whole cameras' FOV as far as possible. In Fig. 11(a), which shows the layout of the ground camera array and the matching result of laser light points between cameras, the red points represent the imaging position of the laser light and the green lines are the matching result among cameras. The camera array self-calibration result of relative poses between two independent cameras is shown in Fig. 11(b), and Fig. 11(c) shows the calibration accurate error analysis of 3D coordinates of light points between vision and GPS data.



(a) The layout of the ground camera array



(b) Cameras self-calibration result



(c) Self-calibration accurate error analysis

Fig. 11. The self-calibration result. (a) The layout of the ground camera array. (b) The camera array self-calibration result. (c) The calibration accuracy comparison of vision and GPS data.

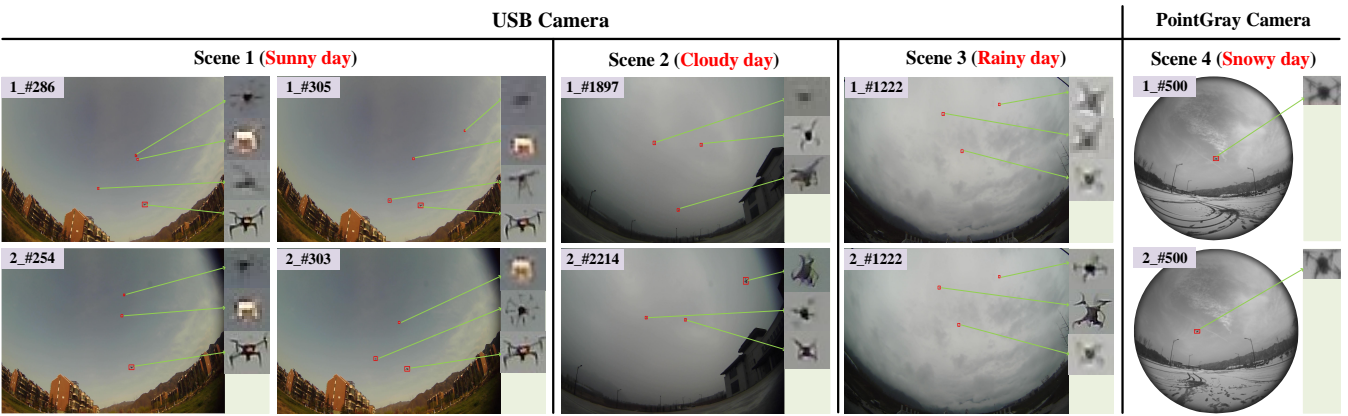


Fig. 12. The detection results of multiple UAVs. The first four columns are photographed using USB camera, which contains three scenes including sunny, cloudy and rainy day. The last column is photographed by pointGrey camera, and which is a snowy day.

### B. Multi-UAV Detection, 3D localization and Tracking

In this section, we focus on the multi-UAV detection, tracking and 3D localization experiments. In order to verify and evaluate the stability of the anti-UAV optical system, we carry out experiments in a variety of camera array structures and different environments(such as sunny, cloudy and even breeze weather) using several UAVs with significant difference in appearance and size.

As we all known, the motor propeller movement is greater than the movement of the fuselage when the vehicles in the hover or low speed flight, as for an independent target, the original ViBe algorithm causes over-segmentation and produces too many small pieces. In order to solve the over-segmentation problem, we do morphological processing and carry out further regional mergers in space, which produces good detection performance. A part of detection results of UAVs are shown in Fig. 12. The first four columns are photographed using USB camera, which contains three scenes including sunny, cloudy and rainy day. The last column is photographed by pointGrey camera is a snowy day. As we can see in the first two frames from the first row in Fig. 12, there are some false detection results in the bottom right of the frame, The removal of false targets is mainly reflected in three aspects. In the process of multi-camera collaborative detection based on the epipolar constrain, the false targets can be removed by the symmetric transfer error; In the process of the camera array vision localization, the false targets can be removed by the space motion track constraints of the UAVs; In the process

of the target tracking, the false targets can be removed by analyzing the motion directions and velocities of the candidate targets. In this way, the target can be detected correctly. And the object of the intermittent detection could also be associated by the following tracking algorithm. There are scale change of UAV and illumination change of experiments as shown in Fig. 12, the proposed method has strong robustness in various challenging scenarios.

We use multi-camera for multi-target synergetic 3D localization. In the experiments, in order to let the UAVs appear in the public view of the cameras, we control the UAVs to fly over the camera. The Fig. 13(a) shows the UAVs fight 3D trajectory and Fig. 13(b) shows the accuracy comparison of GPS and vision localization data. As we can see from the figure, our system with the monitoring capacity of 150 degree wide area. For the structure of the fisheye lens, it can be seen from the experimental results that the positioning accuracy near the center of the camera is obviously higher than that of the surrounding area, the positioning error decreases gradually from far to near for the constraints of the baseline between the cameras. The multiple UAVs tracking experimental results are shown in Fig. 14. The first two rows and the last row represent the tracking results of multiple scenarios of two sensors, respectively. Some false targets are effectively excluded by tracking. The tracking method can effectively track multiple moving targets when exists target crossover. For more insights, we invite the reviewer to take a look at the multimedia demo of our system in the supplementary material.

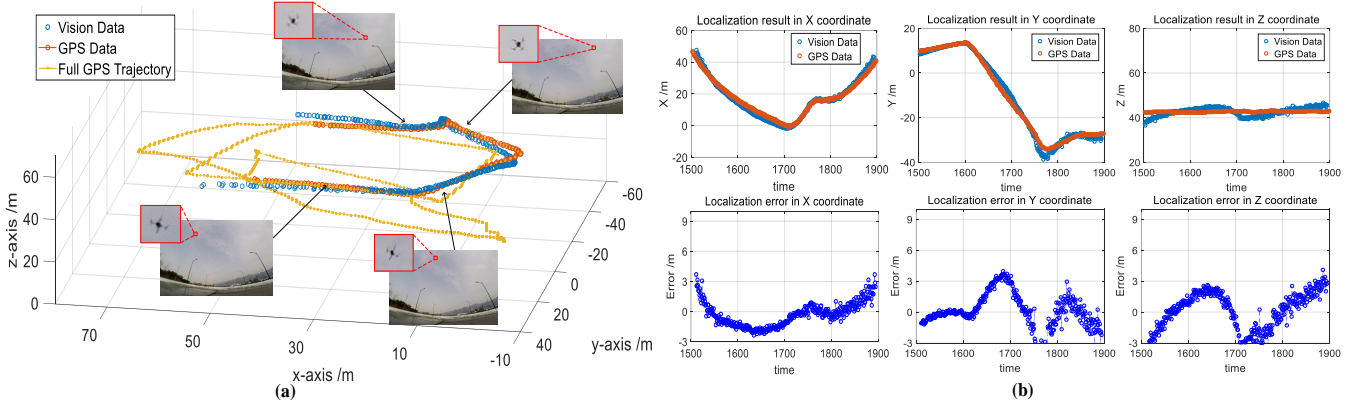


Fig. 13. The localization result and accuracy analysis. (a) Comparison of GPS and vision localization data. (b) The localization results and errors in X, Y and Z coordinates, respectively.

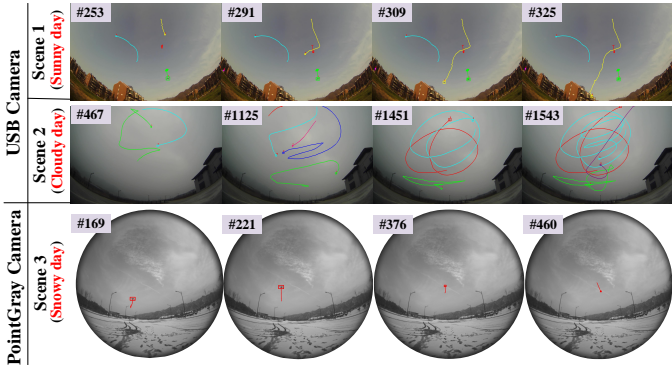


Fig. 14. The tracking results of multiple UAVs. The first two rows and the last row represent the tracking results of multiple scenarios of two sensors, respectively.

## V. CONCLUSIONS

This article firstly constructs a novel real-time panoramic UAV surveillance system based on structure-free fisheye camera array. Compared to the existing UAV surveillance technologies, the fisheye camera array ensures large monitoring FOV, and the free system structure is convenient for rapid deployment and flexible configuration. In addition, we design a robust Near Infrared Laser based self-calibration module and algorithm for arbitrary layout of camera array without any other markers, especially in the environment with low texture or solid color background. And finally, we design an intelligent multi-UAV fast detection, 3D localization and tracking algorithm, which effectively copy with the issues of the scale changes and the interleaving of UAVs during the flight. The system has been tested in various challenging scenarios, include multiple UAVs with significant appearance and scale changes, and even bad weather conditions. Extensive experimental results, both qualitative and quantitative, demonstrate that the robustness and superiority of the proposed system. The experimental results show that the proposed surveillance system can effectively monitor the wide airspace. The future work is to improve the 3D synergetic localization method and tracking algorithm. Further more, we plan to change our static surveillance system to a moving platform, which will have more powerful surveillance capabilities in a larger airspace.

## REFERENCES

- [1] P. Boucher, "Domesticating the drone: the demilitarisation of unmanned aircraft for civil markets," *Science and Engineering Ethics*, vol. 21, no. 6, pp. 1393–1412, 2015.
- [2] R. Altawy and A. M. Youssef, "Security, privacy, and safety aspects of civilian drones: A survey," *ACM Transactions on Cyber-Physical Systems*, vol. 1, no. 2, p. 7, 2017.
- [3] J. F. Vasconcelos, C. Silvestre, P. Oliveira, and B. Guerreiro, "Embedded uav model and laser aiding techniques for inertial navigation systems," *Control Engineering Practice*, vol. 18, no. 3, pp. 262–278, 2010.
- [4] J. Wu, Q. Li, M. He, and F. Zhang, "A terrain model generation method based on 2d plan laser scanner for micro uav autonomous flight," in *Proceedings of the 2012 International Conference on Information Technology and Software Engineering*, pp. 215–225. Springer, 2013.
- [5] S. Weiss, D. Scaramuzza, and R. Siegwart, "Monocular-slam and ndash;based navigation for autonomous micro helicopters in gps-denied environments," *Journal of Field Robotics*, vol. 28, no. 6, pp. 854–874, 2011.
- [6] Q. Fu, Q. Quan, and K.-Y. Cai, "Robust pose estimation for multirotor uavs using off-board monocular vision," *IEEE Transactions on Industrial Electronics*, vol. 64, no. 10, pp. 7942–7951, 2017.
- [7] H. Khosravi and E. Fazl-Ersi, "Trackerbot: A robotic surveillance system based on stereo-vision and artificial neural networks," in *Robotics and Mechatronics (ICROM), 2016 4th International Conference on*, pp. 449–454. IEEE, 2016.
- [8] D. Stepanov and I. Tishchenko, "The concept of video surveillance system based on the principles of stereo vision," in *Open Innovations Association and Seminar on Information Security and Protection of Information Technology (FRUCT-ISPIT), 2016 18th Conference of*, pp. 328–334. IEEE, 2016.
- [9] S. Lange, N. Sünderhauf, P. Neubert, S. Drews, and P. Protzel, "Autonomous corridor flight of a uav using a low-cost and light-weight rgbd camera," in *Advances in Autonomous Mini Robots*, pp. 183–192. Springer, 2012.
- [10] A. Bachrach, S. Prentice, R. He, P. Henry, A. S. Huang, M. Krainin, D. Maturana, D. Fox, and N. Roy, "Estimation, planning, and mapping for autonomous flight using an rgbd camera in gps-denied environments," *The International Journal of Robotics Research*, vol. 31, no. 11, pp. 1320–1343, 2012.
- [11] K. Berger, R. Voorhies, and L. Matthies, "Incorporating polarization in stereo vision-based 3d perception of non-lambertian scenes," in *SPIE Defense+ Security*, pp. 98370P–98370P. International Society for Optics and Photonics, 2016.
- [12] Y. Gui, P. Guo, H. Zhang, Z. Lei, X. Zhou, J. Du, and Q. Yu, "Airborne vision-based navigation method for uav accuracy landing using infrared lamps," *Journal of Intelligent and Robotic Systems*, vol. 72, no. 2, pp. 197–218, 2013.
- [13] C. Martínez, P. Campoy, I. Mondragón, and M. A. Olivares-Méndez, "Trinocular ground system to control uavs," in *Intelligent Robots and Systems, 2009. IROS 2009. IEEE/RSJ International Conference on*, pp. 3361–3367. Ieee, 2009.
- [14] D. Pebranti, F. Kendoul, S. Azrad, W. Wang, and K. Nonami, "Autonomous hovering and landing of a quad-rotor micro aerial vehicle by means of on ground stereo vision system," *Journal of System Design and Dynamics*, vol. 4, no. 2, pp. 269–284, 2010.

- [15] T. Furukawa, C. Kang, B. Li, and G. Dissanayake, "Multi-stage bayesian target estimation by uav using fisheye lens camera and pan/tilt camera," in *Intelligent Robots and Systems (IROS), 2017 IEEE/RSJ International Conference on*, pp. 4167–4172. IEEE, 2017.
- [16] A. Perez-Yus, G. Lopez-Nicolas, and J. Guerrero, "A novel hybrid camera system with depth and fisheye cameras," in *IAPR International Conference on Pattern Recognition (ICPR)*, 2016.
- [17] W. Gao and S. Shen, "Dual-fisheye omnidirectional stereo," in *Intelligent Robots and Systems (IROS), 2017 IEEE/RSJ International Conference on*, pp. 6715–6722. IEEE, 2017.
- [18] A. Gupta, D. Bessonov, and P. Li, "A decision-theoretic approach to detection-based target search with a uav," in *Intelligent Robots and Systems (IROS), 2017 IEEE/RSJ International Conference on*, pp. 5304–5309. IEEE, 2017.
- [19] J. Moreau, S. Ambellouis, and Y. Ruichek, "Fisheye-based method for gps localization improvement in unknown semi-obstructed areas," *Sensors*, vol. 17, no. 1, p. 119, 2017.
- [20] F. Zhou, X. Chai, X. Chen, and Y. Song, "Omnidirectional stereo vision sensor based on single camera and catoptric system," *Applied Optics*, vol. 55, no. 25, pp. 6813–6820, 2016.
- [21] W. Kong, D. Zhang, X. Wang, Z. Xian, and J. Zhang, "Autonomous landing of an uav with a ground-based actuated infrared stereo vision system," in *Intelligent Robots and Systems (IROS), 2013 IEEE/RSJ International Conference on*, pp. 2963–2970. IEEE, 2013.
- [22] W. Kong, D. Zhou, Y. Zhang, D. Zhang, X. Wang, B. Zhao, C. Yan, L. Shen, and J. Zhang, "A ground-based optical system for autonomous landing of a fixed wing uav," in *2014 IEEE/RSJ International Conference on Intelligent Robots and Systems*, pp. 4797–4804. IEEE, 2014.
- [23] T. Yang, G. Li, J. Li, Y. Zhang, X. Zhang, Z. Zhang, and Z. Li, "A ground-based near infrared camera array system for uav auto-landing in gps-denied environment," *Sensors*, vol. 16, no. 9, p. 1393, 2016.
- [24] O. Barnich and M. Van Droogenbroeck, "Vibe: A universal background subtraction algorithm for video sequences," *IEEE Transactions on Image processing*, vol. 20, no. 6, pp. 1709–1724, 2011.